Polarization issues in nanophotonic devices

Jeff F. Young
Department of Physics and Astronomy,
Advanced Materials and Process Engineering Laboratory,
Stuewart Blusson Quantum Matter Institute
University of British Columbia, Vancouver, Canada

The Team

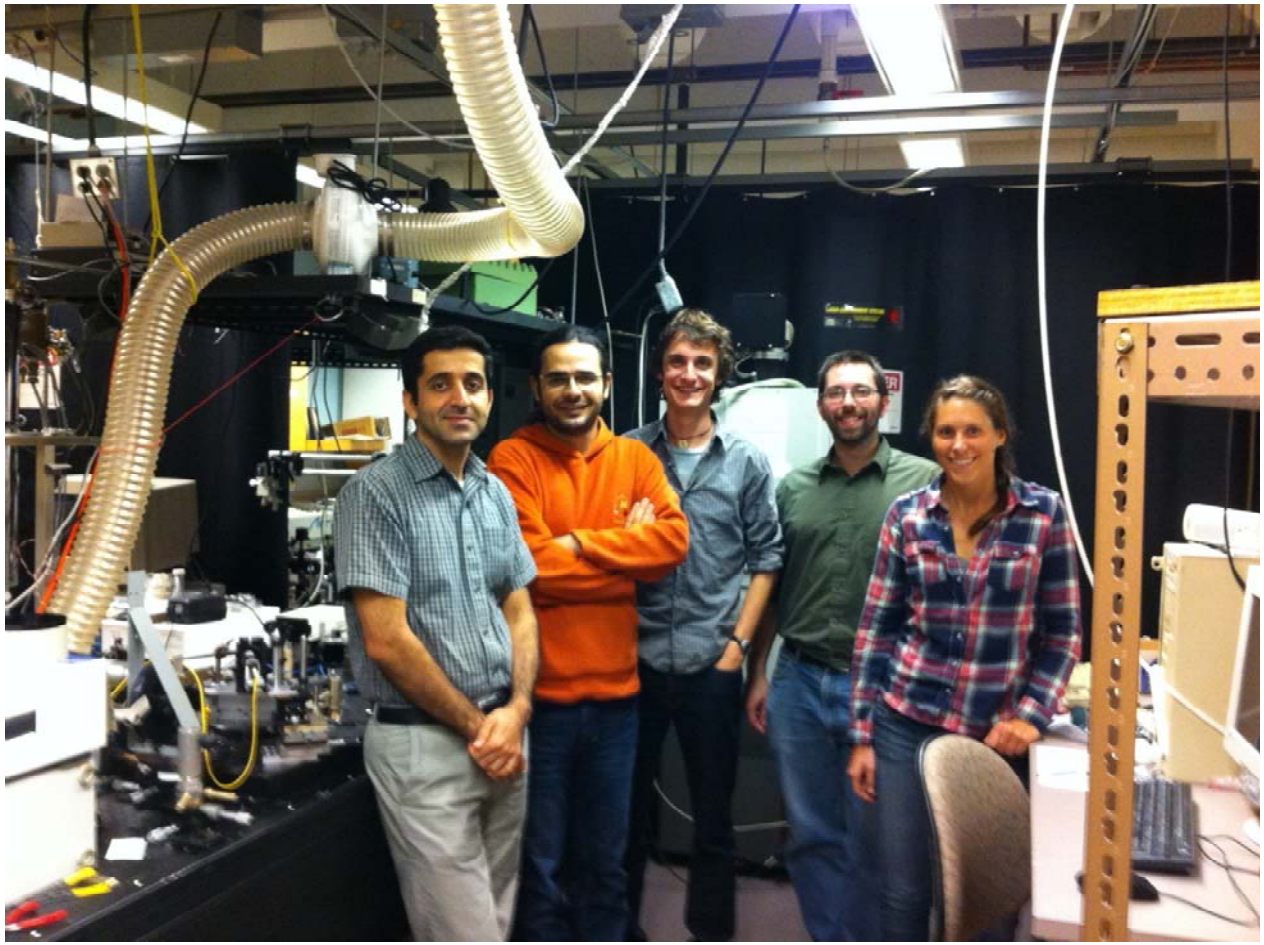

Motivation for our nanophotonics program

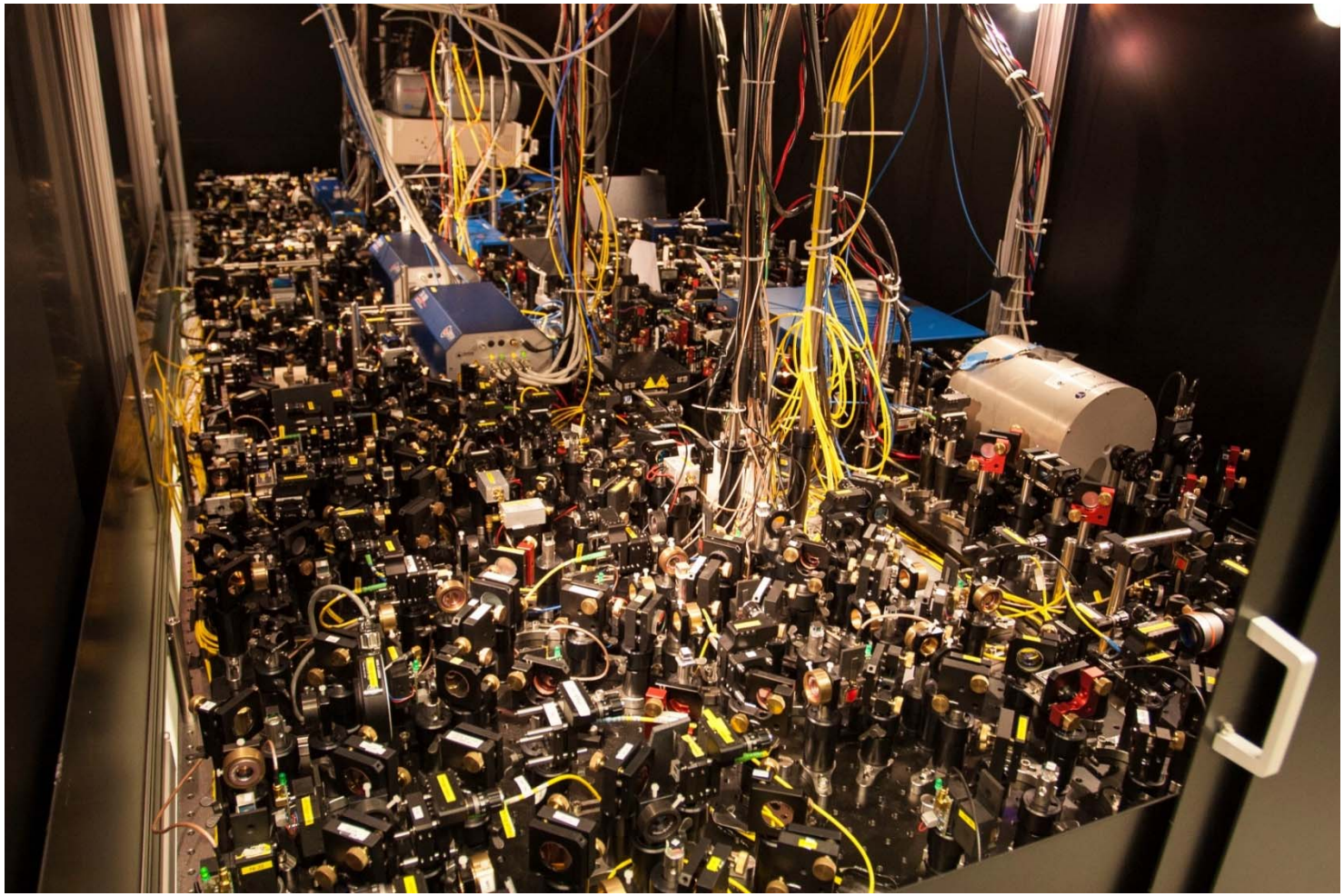

http://www.quantum-munich.de/media/higgs-near-absolute-zero/

Motivation (con't)

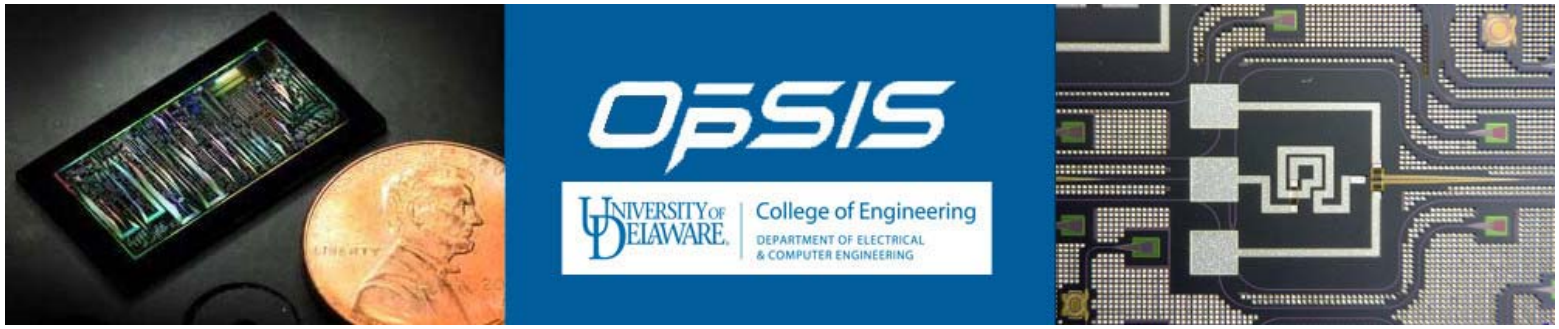

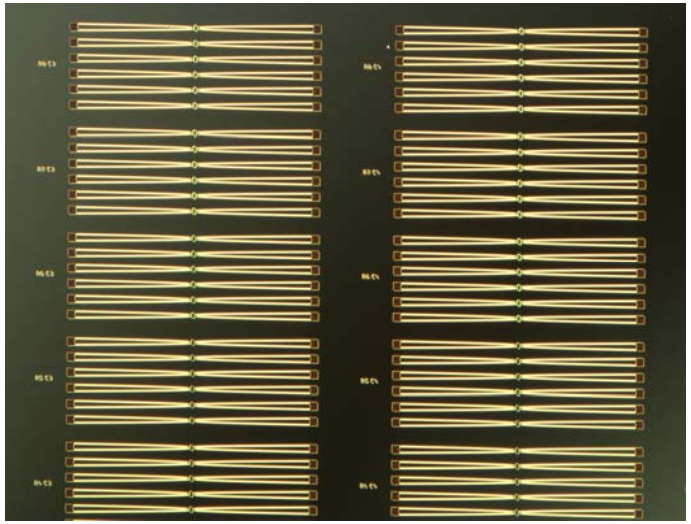

~ 1 mm

~ 100 μm

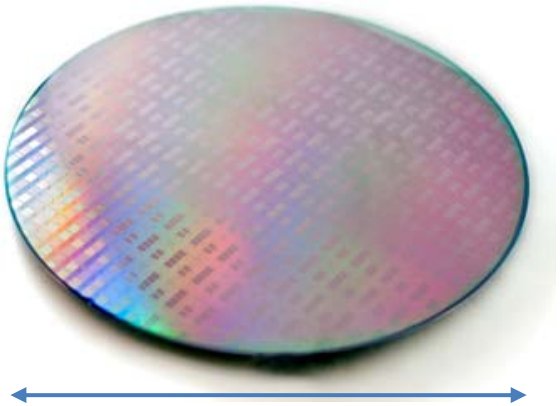

~ 200 mm

Key Elements that Need to be Integrable

- Single and/or Entangled Photon Sources
  - Heralded
  - On-demand
- Single photon Detectors
  - High efficiency
  - Low dark counts
  - fast

Superconducting Nanowire Single Photon Detectors

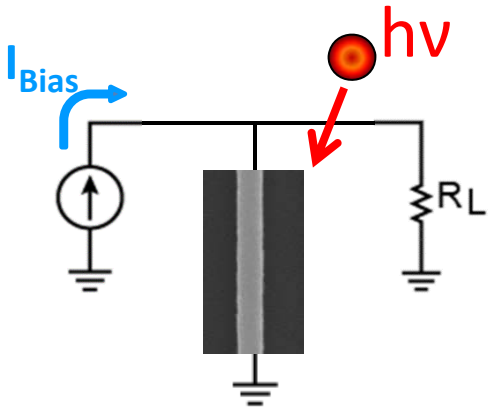

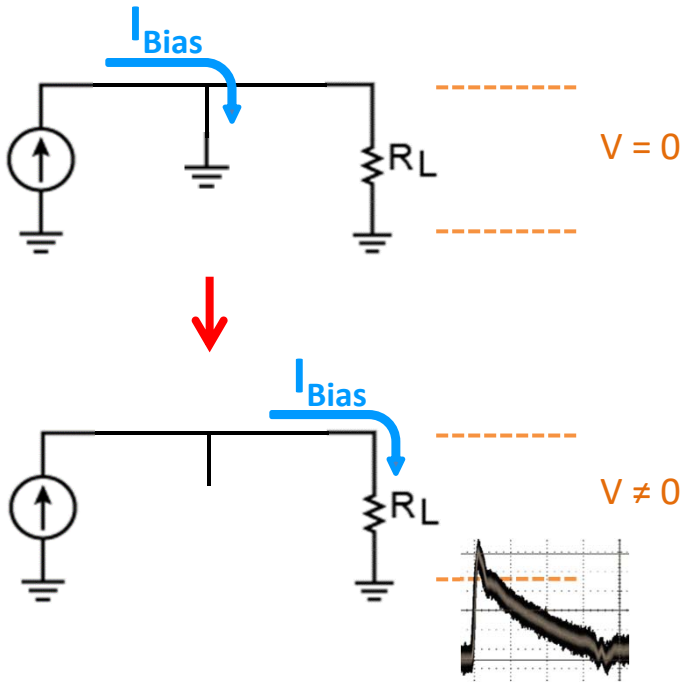

Typical Meandering Implementation:

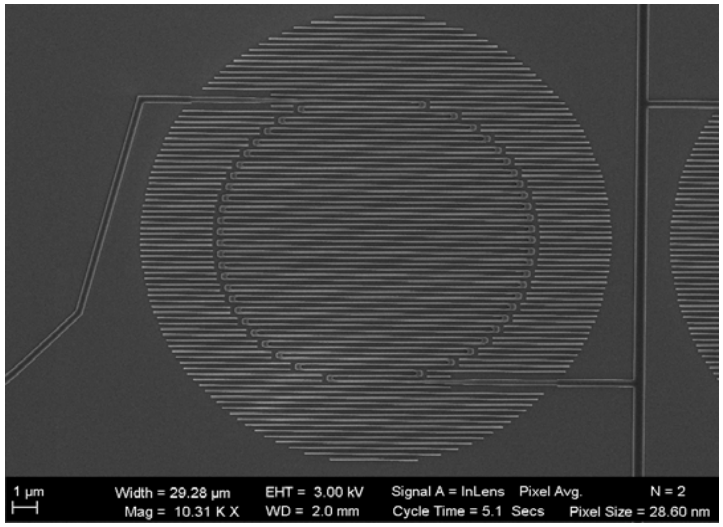

- NbN, NbTiN, Nb
- Few nm Thick
- About 100nm Wide

Concept for integration & enahanced performance:

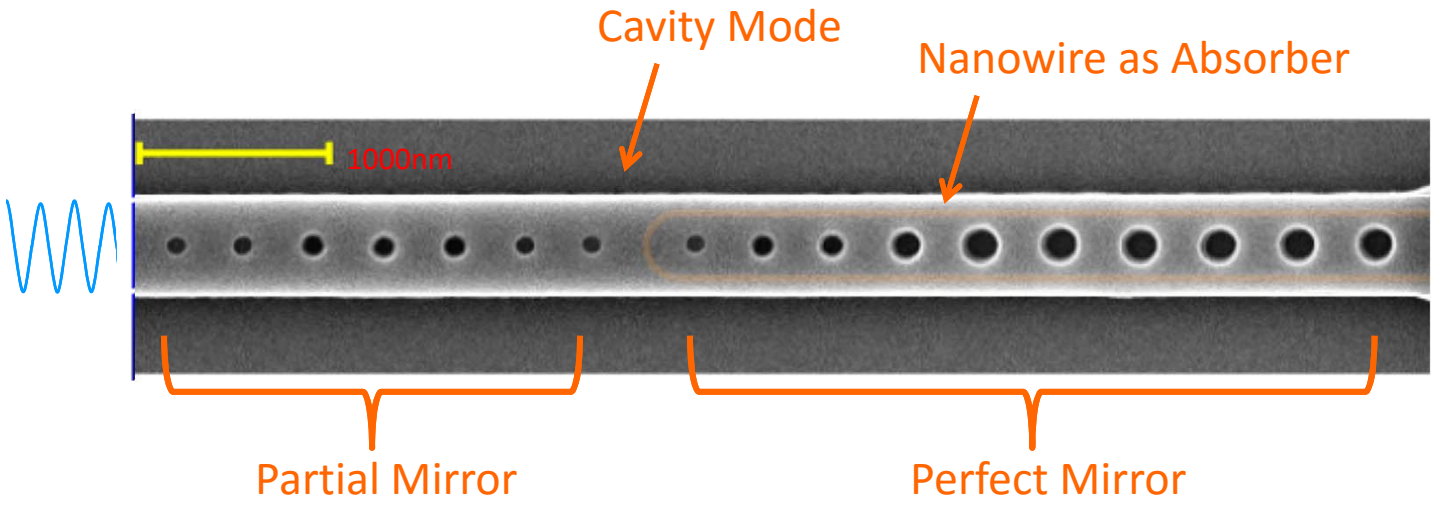

Ideally: $\tau_{MIRROR} = \tau_{ABS}$ ➔ $P_{ABS} = P_{INCIDENT}$

Practically: $Q_{MIRROR} = Q_{ABS} << Q_{SCAT}$ ➔ $Q \cong 0.5Q_{ABS} = 0.5Q_{MIRROR}$

➔ $P_{ABS} \cong P_{INCIDENT}$

Realization:

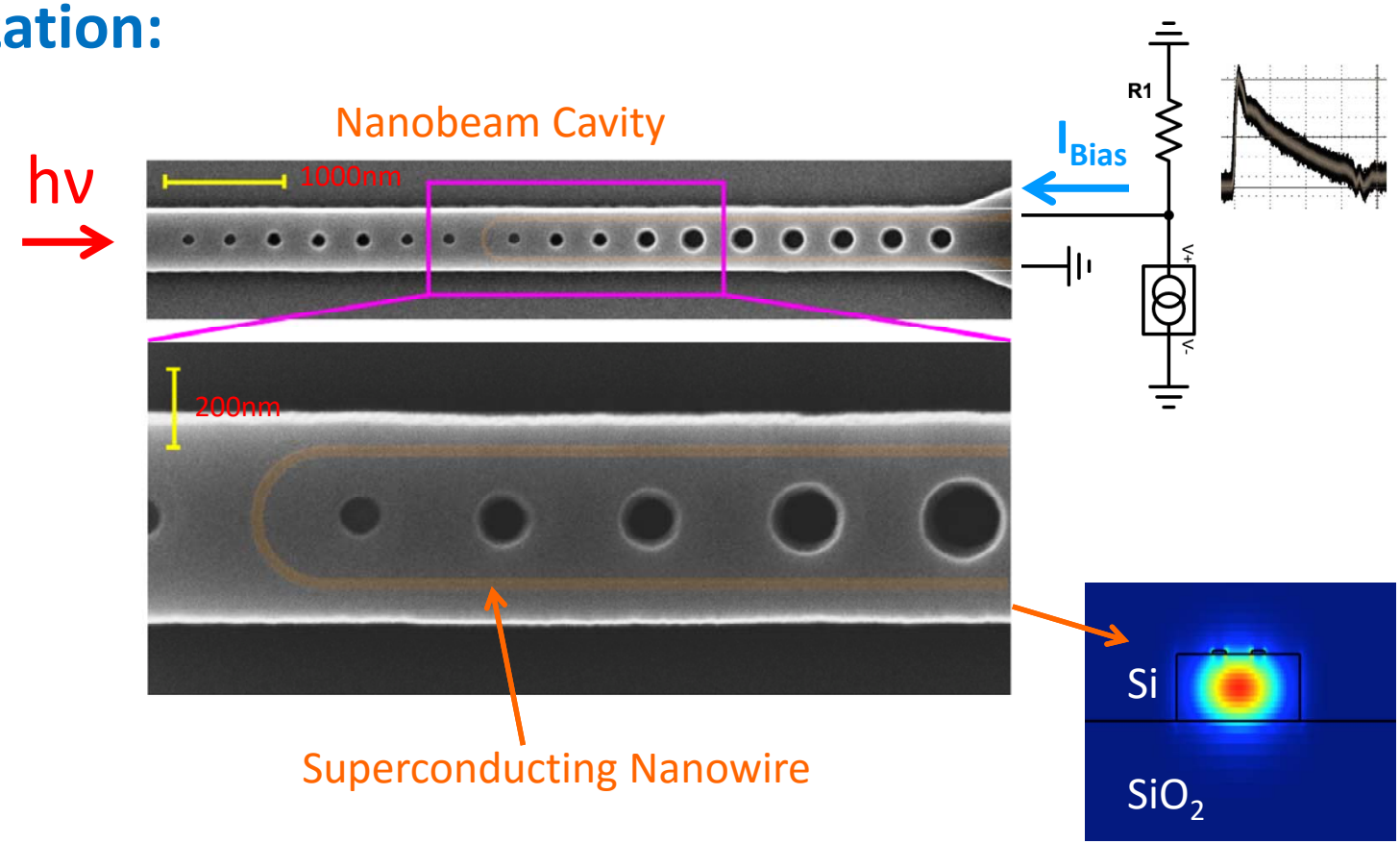

SOI Waveguide
W=500nm, H=190nm

Characterization - Results:

At 2.05K and $0.9I_C$:

Efficiencies vs wavelength

Photon Count Rate (PCR)
Background Count Rate (BCR)
Rate of incident photons(R_{Ph})

$QE\eta_C = (PCR\text{-}DCR)/R_{Ph}$

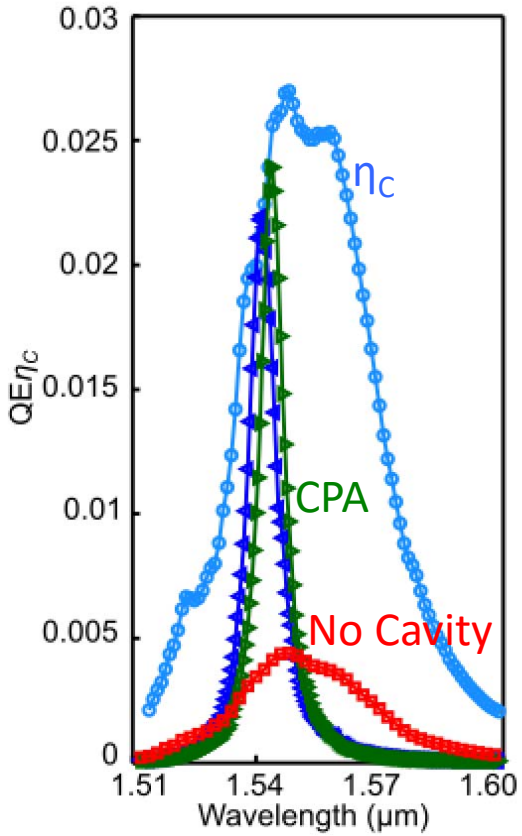

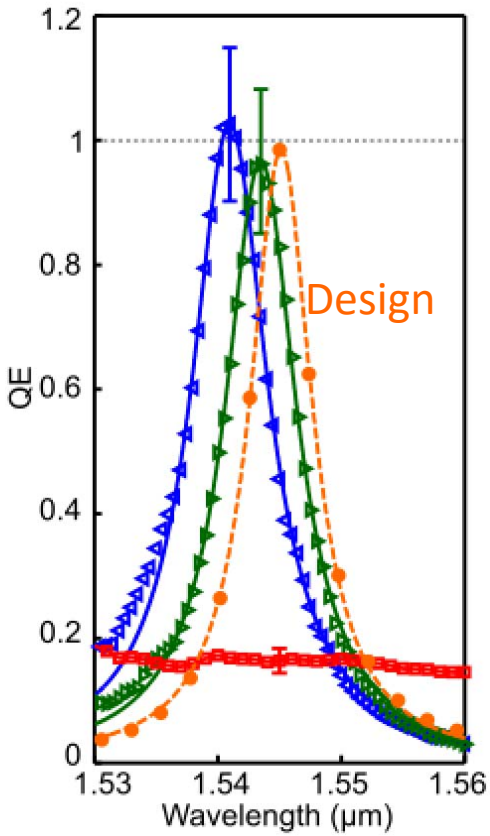

Nature Communications, 6:2041-1723 (2015)

Characterization - Results:

At 2.05K and peak efficiency wavelength:

For CPA detectors

Saturate to 104% and 99%

At $0.9I_C$: 102±8% and 97±8%

At $0.9I_C$: DCR=0.1Hz

For 57.2um no cavity

Saturate to 92%

At $0.9I_C$: ~82%

At $0.9I_C$: DCR=1.1Hz

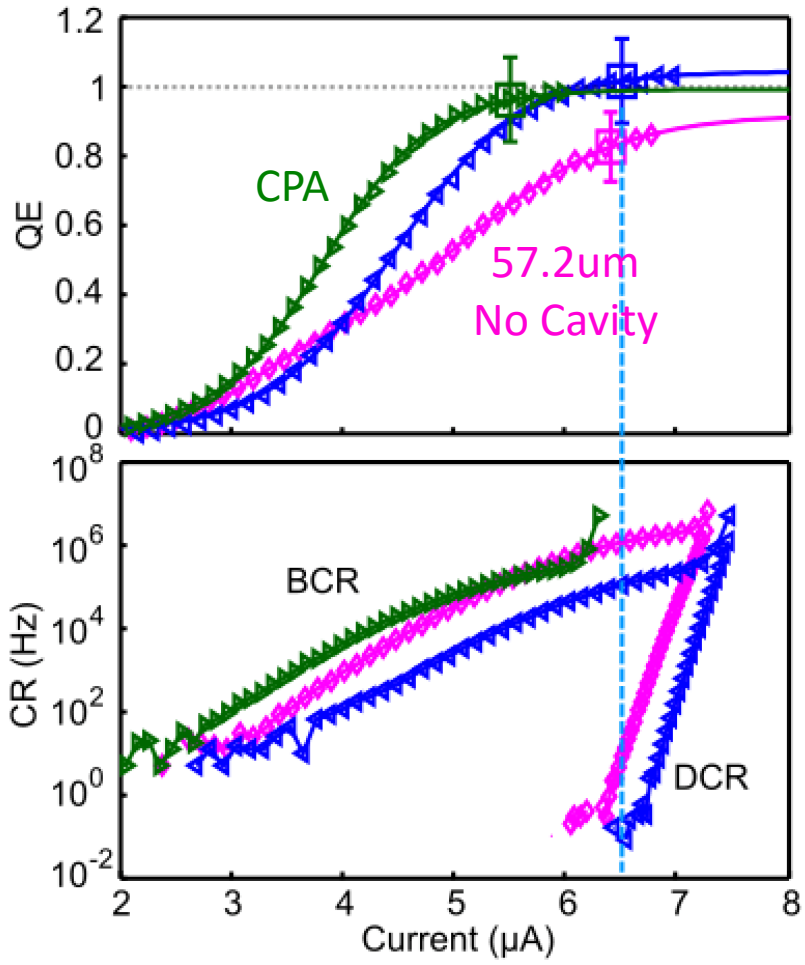

Characterization - Results:

Electronic Jitter:
$2.355\sigma_n/K=53ps$

53ps >> ~15ps >> 0.23ps

Estimated jitter > 53ps

Intrinsic Jitter?

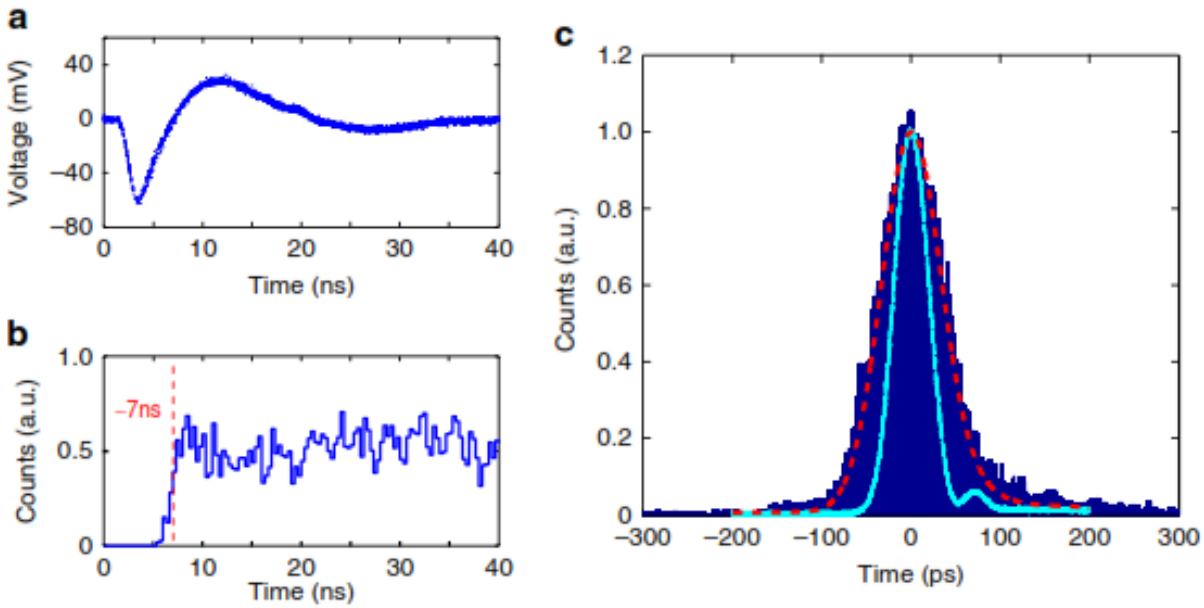

Polarization dynamics

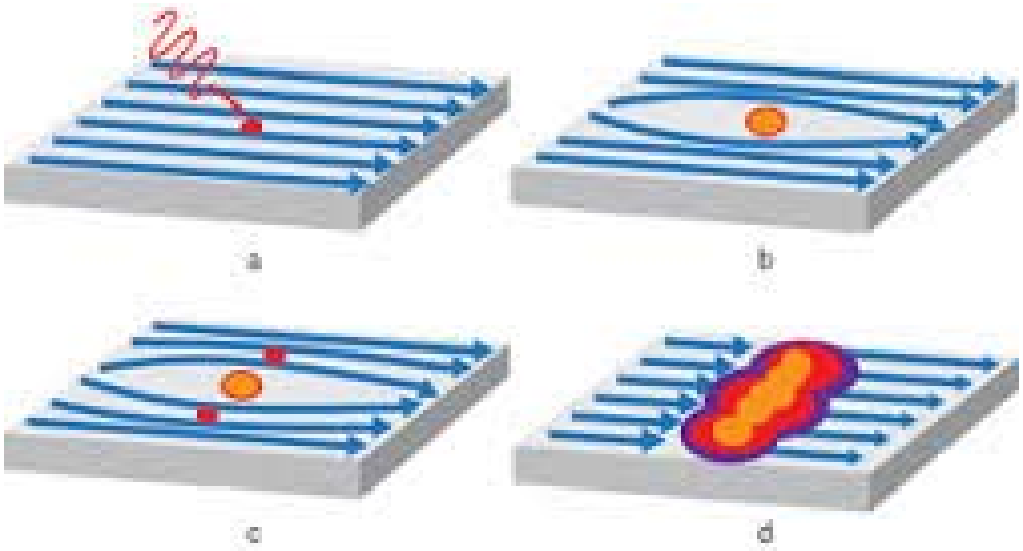

Propagation to readout circuit

Image: MIT Lincoln Labs

Issues

- Microscopic basis for ε used in absorption calculations of 8 nm x 35 nm etched superconductor
- Polarization dynamics associated with spreading hot spot, phase transition, and propagation to circuit

On-Demand Single Photon Source

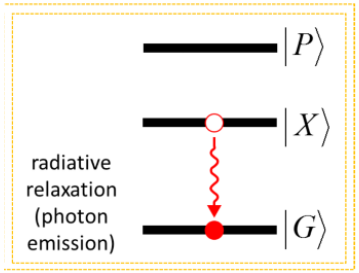

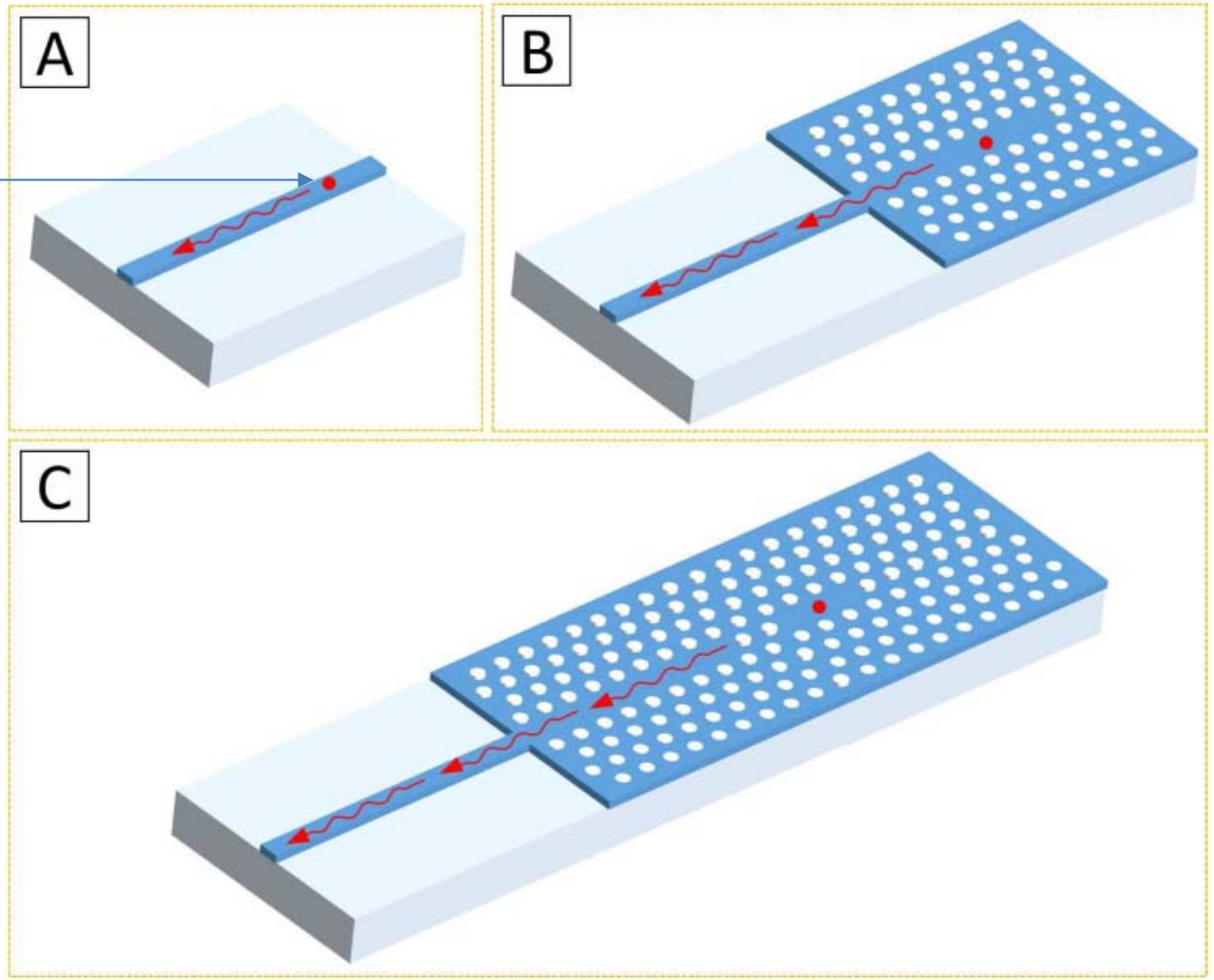

Implementation in Silicon Circuit

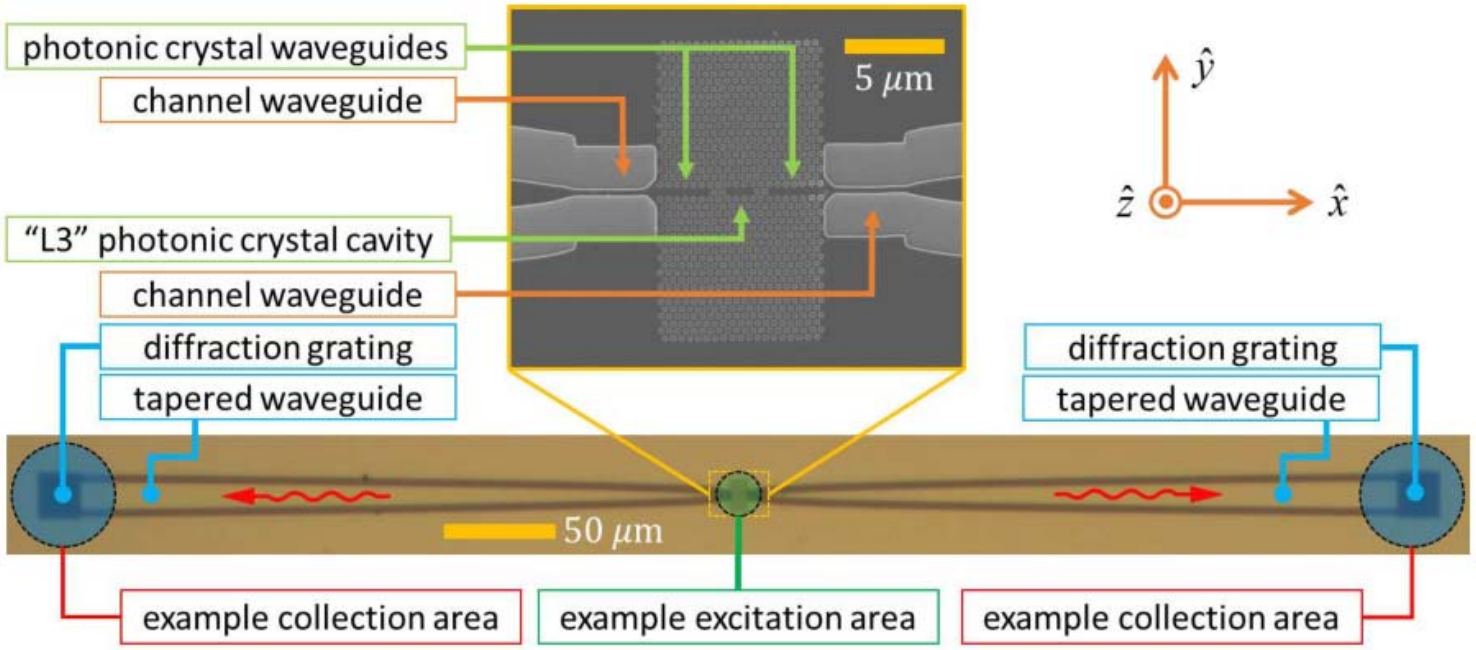

Opt. Exp. **20**, 10453, (2012)

Antinode structure

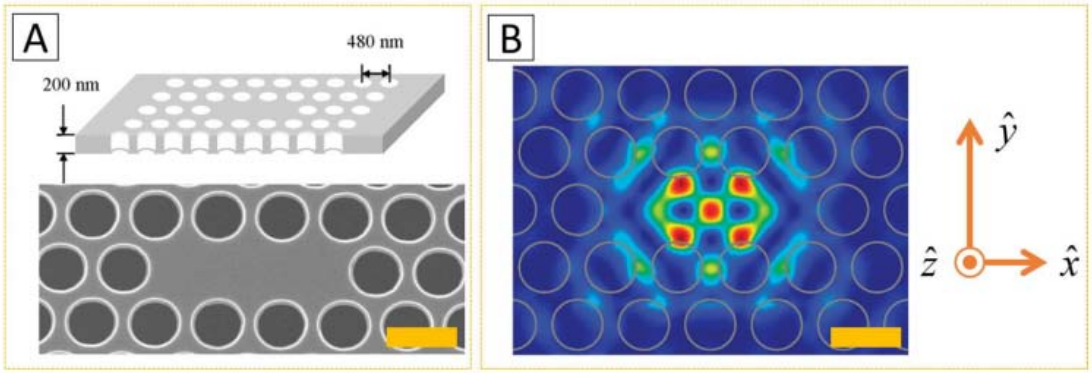

Figure 2.1: (A): Schematic and scanning electron micrograph of an "L3" microcavity. (B): Fundamental in-gap cavity mode electric field intensity at the silicon-air interface, with etched holes outlined. Axes originate at the L3 slab centroid, and $\hat{z}$ is perpendicular to $\hat{x}$ and $\hat{y}$. Yellow scale bars are 500 nm in length. Figure adapted from [165].

Complex dielectric environment

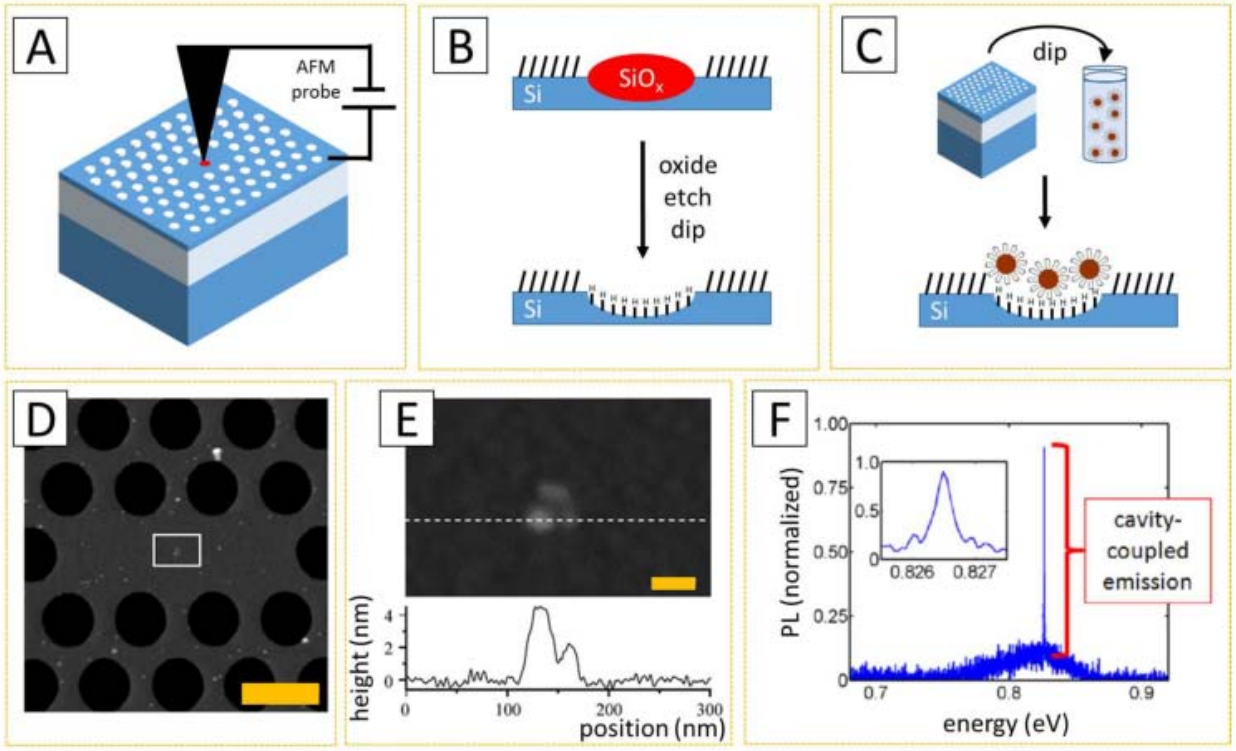

Key Factors

Driving Field Strength

- strong scattering
- ~ 0.1 E_{inc}^2

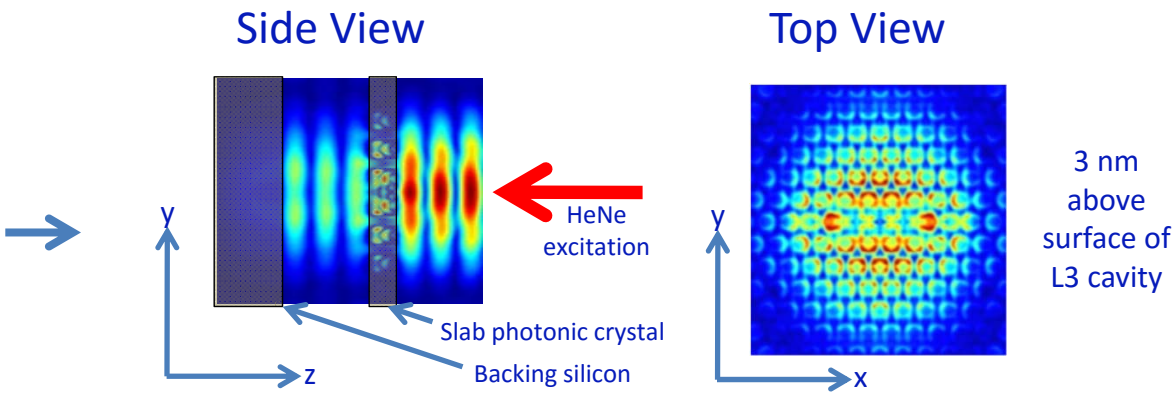

Depolarization
(ε_{NP}~ 20 + 20i)

Effective oscillator strength referenced to absolute absorption in solution:

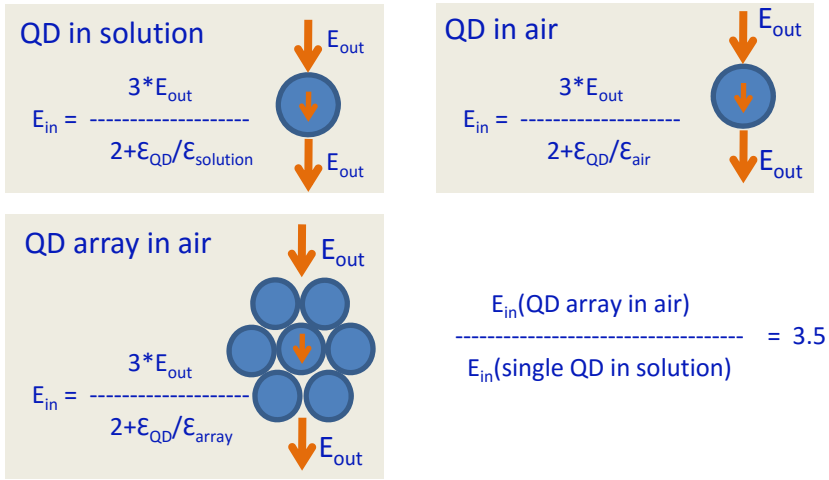

$$\frac{E_{in}(\text{QD array in air})}{E_{in}(\text{single QD in solution})} = 3.5$$

I. Moreels et al., AC Nano (2009).

The emitters

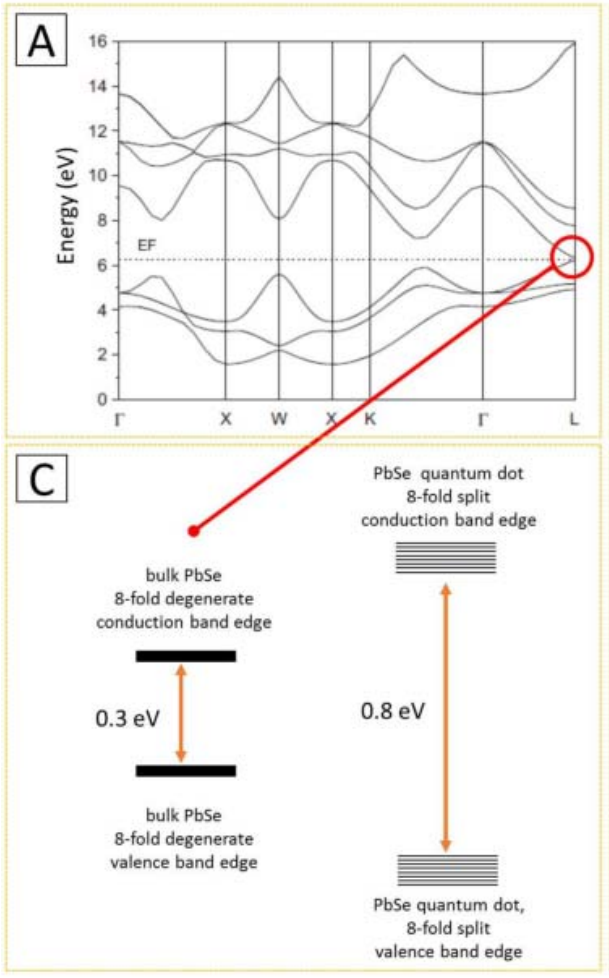

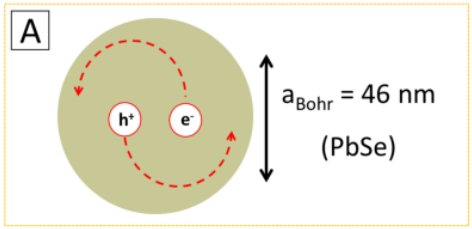

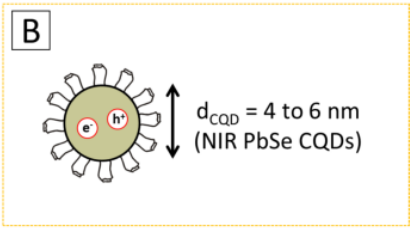

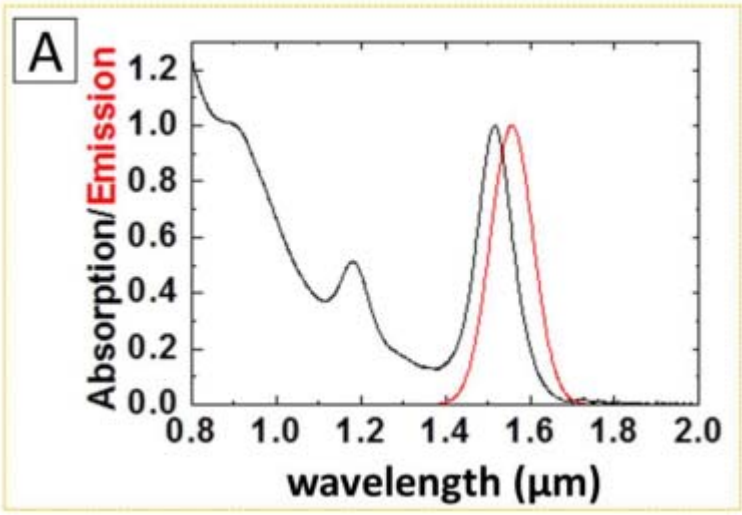

Excitonic transitions (theory)

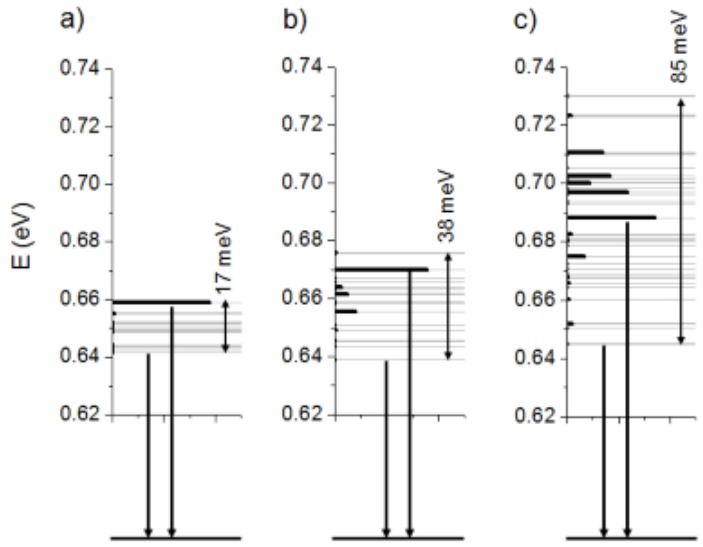

FIG. 5. Dipole matrix elements of optical excitonic transitions for the lowest 64 state excitonic manifold in PbSe dots of 4.3 nm diameter, for a range of asymmetry: (a) reproduced from Fig. 2(b) for clarity, a sphere centered on the long Pb-Se diagonal, (b) a sphere centered on Se atom, (c) ellipsoid of 12 by 12 by 14 half-lattice constants, centered on Se. Thin grey lines show the energies of all transitions while the thick black bars show the relative values of the transition dipole moments.

In contrast to previous calculations [11], however, we find that the electron-hole shell is very sensitive to the geometrical structure of the dot, e.g., the choice of the dot center on cation, anion or between them, the radius of the dot, and deviations from the ideal spherical shape. Depend-

The optical transitions involve creation of electrons and holes as indicated in Fig. 2(a). With 8 states in the conduction band and 8 states in the valence band there are 64 possible electron-hole configurations. The exciton Hamiltonian in the space of electron-hole configurations is constructed using the single particle spectrum of Fig. 2(a) and Coulomb matrix elements computed using the QNANO code. In computation of the Coulomb matrix elements, a distance-dependent dielectric constant is used, with $\epsilon_{\mathrm{on-site}} = 1$ and $\epsilon_{\mathrm{long-range}} = 10$ corresponding to the effective dielectric constant of the film.

Voznyy, Hawrylak

None consistent with experiment(s)

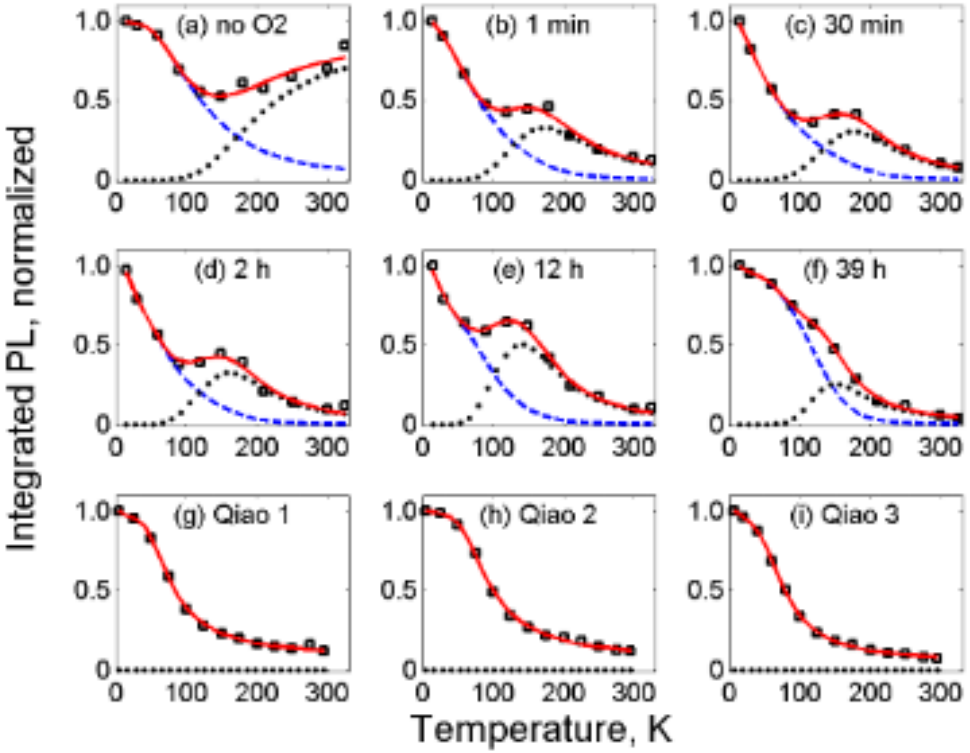

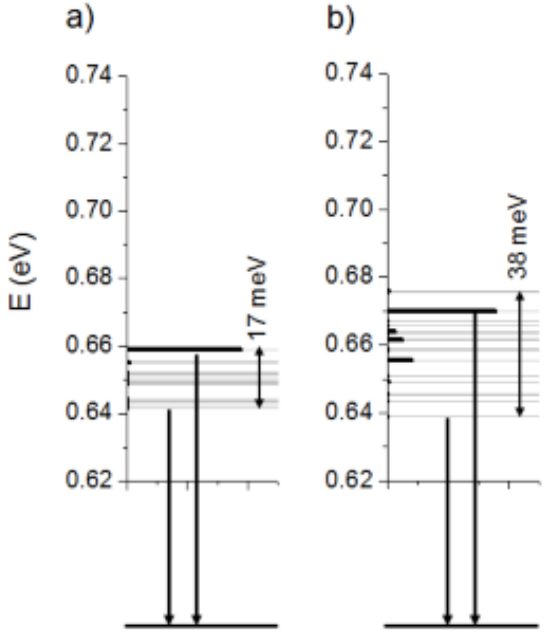

Phys. Rev. B **89**, 045139 (2014)

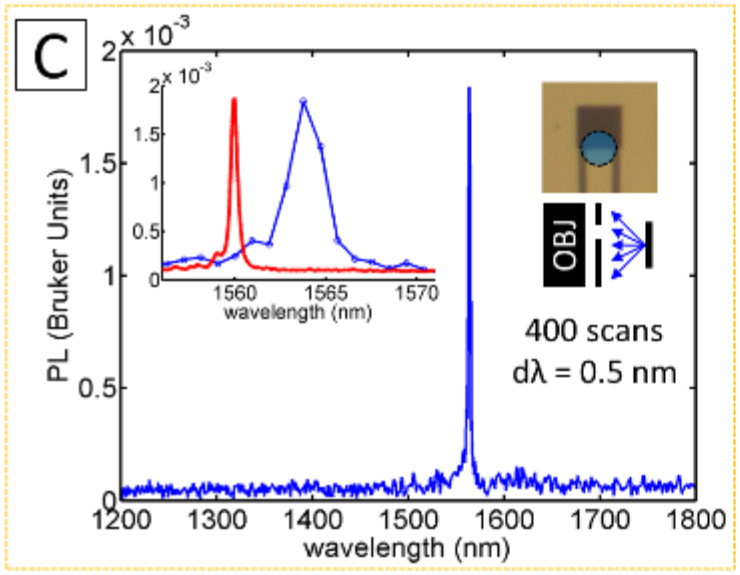

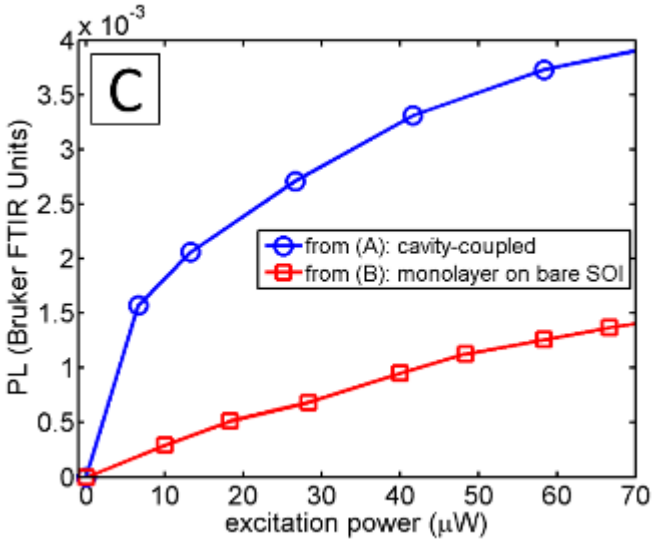

Cavity-coupled

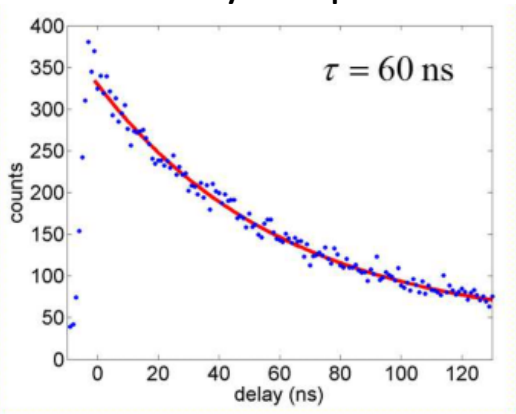

No cavity

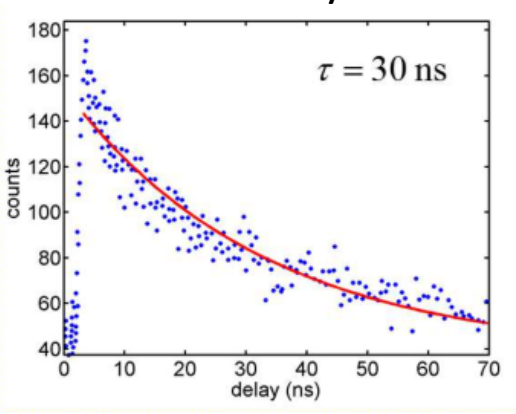

No cavity

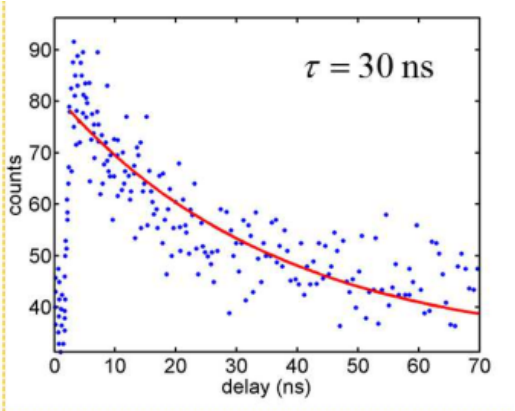

Purcell enhancement

Issues

- Accurate local field calculations (non-resonant response) for high ε, ~ 5 nm nanoparticle ensembles in photonic circuits
- Accurate bandstructure, oscillator strength and exciton spectra of same (resonant response)

PHYSICAL REVIEW B **90**, 125115 (2014)

Linear response of crystals to electromagnetic fields: Microscopic charge-current density, polarization, and magnetization

Sylvia D. Swiecicki* and J. E. Sipe
Department of Physics, University of Toronto, Toronto, Ontario, Canada M5S 1A7
(Received 24 April 2014; revised manuscript received 21 August 2014; published 8 September 2014)

We present an electrodynamic approach to the description of the linear response of solids to electromagnetic fields. For time and spatially varying applied fields we solve the dynamical equations satisfied by the gauge-invariant Green function and find microscopic charge and current densities that result in a form allowing for an easy construction of the multipole expansion of applied fields. Restricting ourselves to static and uniform electric and magnetic fields, we construct microscopic expressions for polarization and magnetization fields associated with each lattice site. The approach is in the spirit of the Power-Zienau-Wooley (PZW) treatment but generalized to account for the motion of the charge between lattice sites. We show that the macroscopic polarization and magnetization can be understood as the spatial average of the generalized PZW microscopic fields.

Contents lists available at ScienceDirect

Annals of Physics

journal homepage: www.elsevier.com/locate/aop

Gauge-invariant Green function dynamics: A unified approach

Sylvia D. Swiecicki *, J.E. Sipe

Department of Physics and Institute for Optical Sciences, University of Toronto, 60 St. George Street, Toronto, Ontario, Canada M5S 1A7

ABSTRACT

We present a gauge-invariant description of Green function dynamics introduced by means of a generalized Peierls phase involving an arbitrary differentiable path in space–time. Two other approaches to formulating a gauge-invariant description of systems, the Green function treatment of Levanda and Fleurov [M. Levanda, V. Fleurov, J. Phys.: Condens. Matter 6 (1994) 7889] and the usual multipolar expansion for an atom, are shown to arise as special cases of our formalism. We argue that the consideration of paths in the generalized Peierls phase that do not lead to introduction of an effective gauge-invariant Hamiltonian with polarization and magnetization fields may prove useful for the treatment of the response of materials with short electron correlation lengths.